Journal of Nuclear Materials 442 (2013) 270–281

Contents lists available at ScienceDirect

Journal of Nuclear Materials

journal homepage: www.elsevier.com/locate/jnucmat

Atom probe tomography study of alloying element distributions in Zr alloys and their oxides

Yan Dong [a], Arthur T. Motta [b], Emmanuelle A. Marquis [a,*]

[a] Department of Materials Science and Engineering, University of Michigan, Ann Arbor, MI 48109, United States
[b] Department of Mechanical and Nuclear Engineering, Penn State University, University Park, PA 16802, United States

ARTICLE INFO

Article history:
Received 10 June 2013
Accepted 31 August 2013
Available online 8 September 2013

ABSTRACT

A detailed study of alloying element distributions in the metal and oxygen rich regions of corroded Zr alloys and of the phases formed ahead of the oxide front was conducted using atom probe tomography (APT). A consistent sequence of sub-oxide phases is observed ahead of the ZrO_2 oxide front, consisting of (i) a thin layer of equiatomic ZrO (occasionally slightly over and under stoichiometric) (ii) saturated solid solution $Zr(O)_{sat}$, and (iii) a slowly decreasing oxygen profile into the metal. The results also show that the distribution of the alloying elements in the metal is more inhomogeneous than previously thought and that in the oxygen-rich phases enhanced segregation is observed, compared to the metal.

1. Introduction

Zirconium based alloys are widely used as nuclear fuel cladding materials in nuclear power plants because of their low thermal neutron capture cross-section, adequate mechanical behavior and good high temperature corrosion resistance [1]. Yet waterside corrosion and its associated hydrogen pickup remain a major issue for utilizing these alloys in severe fuel duty conditions, especially in pressurized water reactors [2]. Alloys with greater corrosion resistance are required to ensure continued fuel efficiency and reliability as burnup increases.

The key to improvements realized in corrosion resistance over the last decades has been a continuous improvement in alloy performance, brought about by incremental alloy modifications and by the introduction of new alloys such as M5 and ZIRLO, which exhibit much better corrosion performance than Zircaloy-4 in the same corrosion environment [3,4]. The difference between the corrosion performance of different alloys is sought in the differences in the structure of the protective oxides formed on these alloys [2]. Much work has been performed in this area, using various techniques, such as cross sectional transmission electron microscopy (TEM), Raman spectroscopy, microbeam synchrotron radiation diffraction and fluorescence to characterize the structure of the layer, including crystal structure, texture, grain size and morphology, porosity and cracking [5–14]. Various authors have reported on the various oxide phases formed including the specific mixture of monoclinic and tetragonal ZrO_2 observed, columnar grain morphology, etc. [15–20].

The determination of the alloying element distribution and precursor oxide phases has received comparatively less attention. The alloying elemental distributions because of their low concentration and fine spatial resolution are most precisely studied with atom probe techniques. Wadman et al. [21] studied the base Zircaloy-2 using 1D atom probe, but did not benefit from very good statistics. More recently Thuvander et al. [22] reassessed the analysis of minor elements in the same alloy. Hudson et al. [23] performed analysis on oxidized Zircaloy-4, Zr–Nb and ZIRLO using pulsed laser field evaporation. More recently, using the same technique, Sundell et al. [24] and Teijland et al. [25] analyzed in detail solute concentrations in oxidized Zircaloy-2, while Wei et al. [26] analyzed the distribution of Sn in corroded Zr–Nb–Sn alloys with different Sn contents.

Several lower stoichiometry metastable oxide phases are predicted from the phase diagram and have been reported by individual researchers using TEM or microbeam synchrotron radiation diffraction [15,20,27–29]. In particular, detailed studies of the oxide–metal interface found by atom probe tomography (APT) that the lower stoichiometry metastable oxide phase, which according to their measurements is ZrO, was present only at pre-transition stage, disappeared after post-transition [19,20]. More recently, Hutchinson et al. [18] observed a region of varying oxide stoichiometry that extends for more than a hundred nanometers into the oxide beneath the metal–oxide interface. They considered this layer as a barrier layer where transport of oxygen takes place by ionic diffusion with important implications for the oxidation process. A summary of some of these results was presented by Preuss et al. [30].

These precursor layers could affect the corrosion kinetics in two principal ways: by using up oxygen that could have been used to form ZrO_2 they slow down the oxide layer advance and by

* Corresponding author. Tel.: +1 7347648717.
E-mail address: emarq@umich.edu (E.A. Marquis).

0022-3115/$ - see front matter © 2013 Elsevier B.V. All rights reserved.
http://dx.doi.org/10.1016/j.jnucmat.2013.08.055

presenting a different material ahead of the advancing oxide they can affect the oxide corrosion kinetics and, possibly the onset of the oxide transition. For example, it has been proposed that the hardening of the matrix near the oxide makes it difficult for the metal to plastically deform to relieve oxide growth stresses. The presence of these layers has also been shown to correlate with the kinetics of oxidation [16], such that the width of the suboxide layer inversely correlates with the corrosion kinetics. Similar results were seen in the examination of oxides formed in supercritical water corrosion at 500 °C [27]. In that instance much thicker suboxide layers were formed that actually had to be accounted for in order to rationalize the weight gain.

Fig. 1 shows the corrosion weight gain of various Zr alloys as a function of exposure time in 360 °C pure water during an autoclave test. Zircaloy-4 (black diamonds) shows the well-known saturating growth behavior with well-defined periodic transitions. Pure Zr and alloys such as Zr–0.5Cr lose protectiveness right away, while others such as Zr–1.0Cu show gradually increased corrosion rate. One of the alloys studied (Zr–0.4Fe–0.2Cr) showed protective behavior for the whole duration of the test (500 days). It is notable that the alloying content variation between these alloys is very small, and yet their behaviors run the gamut from totally protective to immediately non-protective. From these results it is clear that the alloying elements play a role, as yet to be determined, in the protective character of the oxide layer.

To discern this role it is clear that the alloying element distribution in both the alloy and in the oxide layer could be important. For the metal alloy distribution the majority of alloying elements is in precipitates but a fraction could also be dissolved in the matrix, associated with other alloying elements and microstructure features [31]. Concerning the oxide, questions remain as to which elements might be rejected ahead of the oxide front, and whether segregation occurs to the oxide grain boundaries. Such small elemental variations are best studied by atom probe tomography.

In present study, the microstructure and chemistry of the three regions of greatest interest- the oxide, the oxide–metal interface and the metal bulk- were studied using APT. The characterization was performed on three zirconium alloys with different alloying additions in order to investigate the correlation between the distribution of alloying elements and the development of the oxide layers.

2. Experimental methods

The alloys studied were pure Zr (crystal bar), Zircaloy-4, and Zr–0.4Fe–0.2Cr. The nominal chemical compositions of the alloys were measured by vacuum hot extraction and are given in Table 1. The measurements by APT are comparable to those by HVE, at least for the elements homogeneously distributed over the matrix (which is not the case for Fe and Cr as mentioned below).

Coupons of these alloys were autoclave corroded in 360 °C water following ASTM Practice (G2-88) as part of a previous research project [14,27]. The corrosion behavior was evaluated by measuring the weight gain versus exposure time curve, as shown in Fig. 1. The alloy samples used in this study are listed in Table 2. All of the three samples examined in this study were in the protective regime.

Cross-sectional samples were cut from the oxidized coupons and ground on 1200 grit SiC paper on both cross sectional sides. One side of the sample was polished using successively finer polishing cloth to 0.5 μm diamond. The needle-shaped samples for atom probe tomography were prepared using a focused ion beam (FIB)-based lift-out method, which allowed selective extraction of volumes containing metal/oxide interfaces. APT samples with different orientations of interfaces (either parallel or perpendicular to the needle axis) were fabricated to better investigate both the interface region and the oxygen ingress into metal (Fig. 2). Pt was deposited as protective layer and the standard lift-out procedure was applied [32]. A final 2 kV clean-up procedure was utilized to remove any remaining Pt and to minimize Ga damage.

The lift-out samples were analyzed using a CAMECA LEAP-4000XHR operated in a laser pulsing mode with 200 kHz pulse repetition rate and 70–100 pJ laser energy. The temperature of the specimens was maintained at 50 K while the standing voltage was varied automatically to maintain a detection rate of 0.005 ion/pulse. The collected data was reconstructed and analyzed using the reconstruction software, IVAS 3.6.6. The default value of the image compression factor (3.3) and the evaporation field of Zr (28 V/nm [33]) were selected for reconstruction. The composition measurement was done separately for each phase and a peak decomposition technique was used to deconvolute the Zr^{3+} peak from the O_2^+ peaks, which overlap at 32 mass-to-charge ratio.

3. Results

A total of more than 34 needles were studied from the different regions of the three alloy samples, both in the metal and in the oxide. Most APT datasets contain more than 20 million ions to ensure a good statistics. In this section we report the experimental results obtained on the three alloys examined, from needles fabricated at different locations in the bulk and in or near the oxide layers.

3.1. Solute distribution in bulk alloy (away from oxide scale)

3.1.1. Crystal bar

APT samples taken in the bulk of the alloy, i.e. far away from the oxidized surface (~200 μm), show a generally uniform distribution of Cr without any evidence of clusters or indication of elemental segregation to microstructure features such as grain boundaries or dislocations. No Fe was detected in this volume – note that the detection limit for Fe was about 0.002 at.% (12 wt ppm). Concentration measurements from the APT datasets matched the Zr and Cr concentrations measured using hot vacuum extraction as shown in Table 1. Small amounts of C, O and Al were also detected. The low Fe concentration measured in the matrix is reasonable. The alloy is in a recrystallized state with a final heat-treatment temperature corresponding to an extremely low solubility of Fe in Zr [34]. The reported maximum solubility of Fe in α-Zr is 120 wt ppm (0.02 at.%) at 800 °C and less than 50 wt ppm at temperatures lower than 300 °C [35]. Fe is found to be segregated at

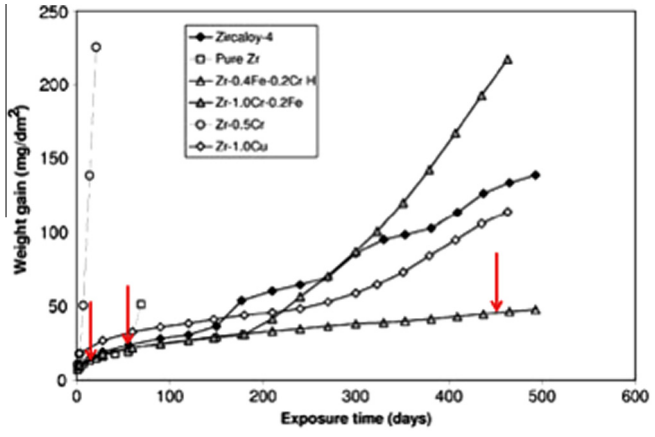

Fig. 1. Corrosion weight gain-exposure time for studied alloys oxidized in 360 °C water [14].